

NEURAL NETWORK APPROACHES FOR PARAMETERIZED OPTIMAL CONTROL

DEEPANSHU VERMA*, NICK WINOVICH[†], LARS RUTHOTTO[‡],
AND BART VAN BLOEMEN WAANDERS[†]

ABSTRACT. We consider numerical approaches for deterministic, finite-dimensional optimal control problems whose dynamics depend on unknown or uncertain parameters. We seek to amortize the solution over a set of relevant parameters in an offline stage to enable rapid decision-making and be able to react to changes in the parameter in the online stage. To tackle the curse of dimensionality arising when the state and/or parameter are high-dimensional, we represent the policy using neural networks. We compare two training paradigms: First, our model-based approach leverages the dynamics and definition of the objective function to learn the value function of the parameterized optimal control problem and obtain the policy using a feedback form. Second, we use actor-critic reinforcement learning to approximate the policy in a data-driven way. Using an example involving a two-dimensional convection-diffusion equation, which features high-dimensional state and parameter spaces, we investigate the accuracy and efficiency of both training paradigms. While both paradigms lead to a reasonable approximation of the policy, the model-based approach is more accurate and considerably reduces the number of PDE solves.

1. INTRODUCTION

We are interested in deterministic, finite-time optimal control problems in which the dynamical system depends on parameters that are unknown or uncertain. Such problems arise in decision-making for complex systems and are prevalent across application domains including physics, engineering, finance, robotics, economics, environmental sciences, and traffic flow [6, 34, 28, 2, 32, 37].

We aim to amortize the solution across multiple parameter uncertainties and obtain a policy that maps the current state and parameter to approximate optimal actions. While this introduces significant offline costs, the policy is fast to evaluate online so that rapid decision-making is enabled. Moreover, our capability supports changes in the parameters over time.

Since an effective policy must depend on the current state of the system and the value of the parameter, amortizing control policies are affected by the curse of dimensionality. When the sum of the dimensions of the state or parameter exceeds approximately four, traditional solution approaches become ineffective. Tackling the curse of dimensionality leads to two critical challenges: First, one needs to determine policies using a high-dimensional function approximator. Motivated by their universal approximation properties, we consider neural networks. Second, identifying the relevant parts of the state space is critical to avoid the infeasibility of globally sampling high-dimensional spaces. Therefore, it is common to limit

2020 *Mathematics Subject Classification.* 35F21, 49M41, 68T07 .

Key words and phrases. Hamilton-Jacobi-Bellman equation, Reinforcement Learning, high dimensional optimal control, PDE constrained optimization, neural networks, policy optimization, actor-critic.

the search to parts of the state space that are likely to be visited when following optimal policies [20, 33].

Given a class of function approximators, we focus primarily on numerical methods for learning effective policies and compare a model-based and a data-driven approach. Our model-based approach approximates the value function of the control problem from which the policy is obtained using a feedback form. The feedback form requires a model of the dynamical system and knowledge of the objective functional. This enables the incorporation of the physics of the system and include known properties of the value function, via the Hamilton-Jacobi-Bellman (HJB) equations, into the training problem. Our data-driven approach uses the framework of actor-critic reinforcement learning to decouple the networks for the policy (i.e., the actor) and the value function (i.e., the critic) and trains both networks purely from observations. Both approaches are intimately related through the underlying control theory, especially Pontryagin’s maximum principle theory and HJB equations.

To compare the accuracy and efficiency of both approaches, we implement a model problem motivated by control of contaminant transport. Here, the state is governed by the two-dimensional advection-diffusion partial differential equation (PDE). The objective is to prevent a contaminant originating at a source location from reaching a target region by controlling the location of a sink. Uncertain parameters in this case consist of different scenarios for the source location and the velocity field. Since both the state and the parameter are infinite-dimensional, the problem is well-suited to create high-dimensional problem instances through discretization. Both the state and the parameters are infinite-dimensional and therefore motivate high-dimensional problems after discretization.

Our main contributions and observations are summarized as follows:

- We extend the optimal control approaches from [27] to parametric control problems, which leads to a considerable increase in the dimensionality of the problem.
- We provide a direct comparison of the OC and RL approaches and including resective sub-optimality. For the parameterized OC approach, this experiment increases the dimension from around 100 in [27] to about 1000 (see section 6).
- We observe in our experiments that the OC approach achieves more accurate policies with fewer simulations (20x less) of the dynamical system.

The remainder of the paper is organized as follows: Section 2 introduces the parametric OC problem and provides a brief background on OC theory that informs our approaches. Section 3 discusses related approaches for learning amortized policies. Section 4 presents our neural network approach for computing the value function. Section 5 revisits key RL concepts, laying the groundwork for employing Proximal Policy Optimization (PPO) and Twin Delayed Deep Deterministic Policy Gradients (TD3) algorithms in policy approximation. Section 6 conducts a comprehensive numerical assessment of both the neural-HJB and RL approaches, employing PDE-based dynamics. Finally, Section 6.4 provides a thorough discussion of results, highlighting the strengths and limitations of the proposed methodologies.

2. PARAMETERIZED OPTIMAL CONTROL PROBLEM

We consider a family of deterministic, finite horizon optimal control problems of the form

$$(2.1a) \quad \min_{\mathbf{u} \in U} J(t, \mathbf{x}, \mathbf{u}; \mathbf{y}) := \int_t^T L(s, \mathbf{z}(s), \mathbf{u}(s)) ds + G(\mathbf{z}(T)),$$

subject to a nonlinear dynamical constraint

$$(2.1b) \quad d_s z(s) = f(s, z(s); \mathbf{y}) + g(s, z(s); \mathbf{y}) \mathbf{u}(s), \quad s \in (t, T]; \quad z(t) = \mathbf{x},$$

where, given a parameter $\mathbf{y} \in \eta$, the functions $f : [0, T] \times \mathbb{R}^d \rightarrow \mathbb{R}^d$ and $g : [0, T] \times \mathbb{R}^d \rightarrow \mathbb{R}^{d \times a}$ model the evolution of the states $\mathbf{z} : [0, T] \rightarrow \mathbb{R}^d$ in response to the controls $\mathbf{u} : [0, T] \rightarrow U \subset \mathbb{R}^a$. The initial state of the system is denoted as $\mathbf{x} \in \mathbb{R}^d$, and the initial time is represented by $t \in [0, T]$. The function $L : [0, T] \times \mathbb{R}^d \times \mathbb{R}^a \rightarrow \mathbb{R}$ represents the running cost, and $G : \mathbb{R}^d \rightarrow \mathbb{R}$ represents the terminal cost in the control objective eq. (2.1a).

We assume that f, L, G, U are sufficiently regular (see [39, Chapter 2] for a list of assumptions)

We aim to determine an optimal control (policy) amortized over the parameters $\mathbf{y} \in \eta$ that minimizes the overall cost. In particular, given a specific parameter \mathbf{y} , we seek to find the value function

$$(2.2) \quad \Phi(t, \mathbf{x}; \mathbf{y}) = \inf_{\mathbf{u} \in U} J(t, \mathbf{z}, \mathbf{u}; \mathbf{y}) \quad \text{s.t.} \quad \text{eq. (2.1b)},$$

which represents the minimum cost-to-go for any initial state (t, \mathbf{x}) . The control \mathbf{u}^* for this minimum value is referred to as optimal control, and the corresponding trajectory \mathbf{z}^* is called an optimal trajectory.

The problem eq. (2.1) is typically tackled using local solution methods. These methodologies involve minimizing the cost functional by eliminating the constraints, all while considering a fixed parameter \mathbf{y} . However, these localized strategies necessitate reevaluating the solution each time the \mathbf{y} changes, rendering the previously computed solution obsolete. This clearly highlights the need for devising a control policy that is amortized over the parameters $\mathbf{y} \in \eta$.

Subsequently, we will see that the value function Φ contains complete information about the optimal control, and we can straightforwardly deduce \mathbf{u}^* from Φ . Notably, this connection is not explicitly utilized by RL algorithms during policy approximation. This distinction between the HJB approach and RL is significant, as leveraging the underlying physics of the problem can lead to improved results as presented in section 6.

We now introduce the Hamiltonian, $H : [0, T] \times \mathbb{R}^d \times \mathbb{R}^d \rightarrow \mathbb{R} \cup \{\infty\}$ of the system eq. (2.1), which plays a pivotal role in both OC theory and our numerical approach:

$$(2.3) \quad H(s, \mathbf{z}, \mathbf{p}; \mathbf{y}) = \sup_{\mathbf{u} \in U} \mathcal{H}(s, \mathbf{z}, \mathbf{p}, \mathbf{u}; \mathbf{y})$$

Here $\mathbf{p} : [t_0, T] \rightarrow \mathbb{R}^d$ is referred to as the adjoint or costates of the system, and

$$\mathcal{H}(s, \mathbf{z}, \mathbf{p}, \mathbf{u}; \mathbf{y}) = \mathbf{p} \cdot (f(s, \mathbf{z}; \mathbf{y}) + g(s, \mathbf{z}; \mathbf{y}) \mathbf{u}) - L(s, \mathbf{z}, \mathbf{u}).$$

The Pontryagin maximum principle provides a set of first-order necessary conditions and states that, see [9, Theorem I.6.3], the adjoint, \mathbf{p} , satisfies the adjoint equation. Furthermore, when the value function Φ is differentiable, the adjoint \mathbf{p} and the optimal control \mathbf{u}^* can be derived from Φ using [9, Theorem I.6.2]: for $s \in [t, T]$

$$(2.4) \quad \mathbf{p}(s) = \nabla_{\mathbf{z}} \Phi(s, \mathbf{z}^*(s); \mathbf{y}), \quad \text{and}$$

$$(2.5) \quad \mathbf{u}^*(s, \mathbf{z}^*(s), \nabla_{\mathbf{z}} \Phi(s, \mathbf{z}^*(s); \mathbf{y})) \in \arg \max_{\mathbf{u} \in U} \mathcal{H}(s, \mathbf{z}^*(s), \nabla_{\mathbf{z}} \Phi(s, \mathbf{z}^*(s); \mathbf{y}), \mathbf{u}(s); \mathbf{y}).$$

The eq. (2.5) characterizes optimal control in feedback form, and states that it can be readily computed at any space-time pair, for a given \mathbf{y} , when the value function Φ and $\nabla_{\mathbf{z}} \Phi$ are available. For a thorough exploration of the aforementioned relationships, we refer the readers to [9, 20, 27].

The model-based approach exploits this fundamental relationship to approximate a Φ amortized across diverse parameters \mathbf{y} . This ensures a readily accessible approximate optimal control for each parameter setting. The data-driven approach, on the other hand, is agnostic to this relationship and hence suffers in terms of accuracy.

3. RELATED WORK

This section reviews some closely related approaches for control/policy training. Existing approaches can roughly be grouped by the type of function approximators used and whether they primarily use the model or data during training. Specifically focusing on NNs as function approximators, we distinguish between model-based and data-driven training algorithms.

Model-based approaches, like the one presented by Kang *et al.* [16] adopt a supervised learning approach to learn a closed-form value function. The physics-informed neural networks (PINNs) method [22, 25] integrates the cost functional into the standard PINNs loss for solving OC problems. Other techniques, such as deep-learning-based surrogate models [37, 23] and operator learning methods [35, 13], focus on achieving fast OC solution inference without intensive computations. In [8], an extended PINN approach utilizes Karush–Kuhn–Tucker (KKT) conditions as the loss function. These approaches primarily tackle OC problems with partial differential equations (PDEs) as constraints.

A recent development is the adjoint-oriented neural network method proposed in [38] for parametric OC problems. This method learns the states, adjoints, and control of the system through three different neural networks using a direct-adjoint looping method-type loss. While capable of handling parametric problems simultaneously with random sampling instead of spatial domain discretization, it faces challenges in the presence of changes in initial states or disturbances when following the optimal solution. Moreover, training separate networks introduces computational complexity, limiting the applicability of this approach to less complex problems.

Reinforcement learning (RL) has emerged as a potent data-driven approach and shown success in diverse applications such as robotics, autonomous driving, games, and recommender systems [24, 30, 36, 31, 7, 14, 4]. Its non-intrusive and gradient-free nature make RL suitable for problems lacking well-defined models. However, RL often requires many samples, which are computationally expensive in our setting. The process of hyperparameter tuning in RL algorithms is laborious and computationally expensive, hindering their applicability for parametric dynamics [26, 12, 15, 42, 1]. To overcome these limitations, there is a growing interest in effectively integrating system knowledge to overcome the constraints of data-driven methods for handling complex dynamics. In [40, 41], the authors investigate solving OC problems using actor-critic and policy gradient type methods within the realm of RL. While successful for general OC problems, these methods have limited direct applicability to parametric problems. The main challenge arises from the added complexity introduced by parameters, in addition to the already expensive task of evolving the dynamics over time.

Works closely related to our OC approach include [27, 19, 20], which employ NNs to parameterize the value function and penalize the HJB equation satisfied by the value function.

4. MODEL-BASED APPROACH

In this section, we present our model driven approach, inspired by [27], for approximating the amortized value function of the parameterized OC problem eq. (2.1). The central concept

revolves around utilizing an efficient function approximator to model the amortized value function Φ in eq. (2.2) and subsequently computing the control using the feedback form given by eq. (2.5). The learning adopts an unsupervised approach, akin to RL. The loss function consists of the sum of the expected cost over different parameters, $\mathbf{y} \in \eta$, driving the trajectories and penalty terms that enforce the HJB equations along the trajectories and at the final-time.

4.1. Learning Problem. Let Φ_{θ} denote the approximation of the value function Φ with parameters θ . Ideally, we aim for a choice of θ where Φ_{θ} matches the value function of the corresponding control problem for every given \mathbf{y} . However, this problem suffers from the curse of dimensionality so we resort to an approach which enforces this property in a subset of space-time domain.

To learn the parameters in an unsupervised way (that is, no apriori data for Φ and optimal control trajectories), we approximately solve the minimization problem

$$(4.1) \quad \begin{aligned} \min_{\theta} \mathbb{E}_{\mathbf{y} \sim \eta} \{J(t, \mathbf{z}, \mathbf{u}; \mathbf{y}) + P_{\text{HJB}, \mathbf{y}}(\mathbf{z})\} \\ \text{s.t.} \quad \mathbf{d}_s \mathbf{z} = \mathbf{f}(s, \mathbf{z}(s); \mathbf{y}) + \mathbf{g}(s, \mathbf{z}(s); \mathbf{y}) \mathbf{u}(s), \quad s \in (t, T]; \quad \mathbf{z}(t) = \mathbf{x}. \end{aligned}$$

Here $P_{\text{HJB}, \mathbf{y}}$ penalizes deviations from the HJB PDE satisfied by the value function for each parameter \mathbf{y} . In the learning process, the optimal control is computed through the feedback form provided in eq. (2.5), hence, incorporating the model information.

Exploiting the fact that the value function satisfies the HJB PDE (see [9, Theorems I.5.1, I.6.1]), we guide the approximation of Φ using the penalty term $P_{\text{HJB}, \mathbf{y}}$, defined as:

$$(4.2) \quad \begin{aligned} P_{\text{HJB}, \mathbf{y}}(\mathbf{z}) = & \beta_1 \int_t^T |H(s, \mathbf{z}, \nabla \Phi_{\theta}(s, \mathbf{z}(s); \mathbf{y}); \mathbf{y}) - \partial_s \Phi_{\theta}(s, \mathbf{z}(s); \mathbf{y})| ds \\ & + \beta_2 |G(\mathbf{z}(T)) - \Phi_{\theta}(T, \mathbf{z}(T); \mathbf{y})| + \beta_3 |\nabla_{\mathbf{z}} G(\mathbf{z}(T)) - \nabla_{\mathbf{z}} \Phi_{\theta}(T, \mathbf{z}(T); \mathbf{y})|, \end{aligned}$$

where the relative influence of each term is controlled by the components of $\beta = (\beta_1, \beta_2, \beta_3) \in \mathbb{R}_+^3$.

We further make the following assumption for our model driven approach.

Assumption 4.1. There exists a closed form solution to eq. (2.5), which allow us to write the control \mathbf{u} as a function of $\nabla_{\mathbf{z}} \Phi$, explicitly, i.e.

$$(4.3) \quad \mathbf{u}^*(s, \mathbf{z}^*(s), \nabla_{\mathbf{z}} \Phi(s, \mathbf{z}^*(s); \mathbf{y}); \mathbf{y}) = \arg \max_{\mathbf{u} \in U} \mathcal{H}(s, \mathbf{z}^*(s), \nabla_{\mathbf{z}} \Phi(s, \mathbf{z}^*(s); \mathbf{y}), \mathbf{u}(s); \mathbf{y}),$$

A closed-form solution for the optimal control exists in a wide variety of OC problems [21, 3, 18]. While we do not explicitly demonstrate it in this work, it is worth noting that this assumption can be relaxed to include implicitly defined functions as long as they can be efficiently obtained. This flexibility allows for the modeling of more general convex running costs and enhances the applicability of our approach to a wider range of problems.

The eqs. (4.1) and (4.3) provide a framework for obtaining the optimal control and trajectory based on the value function Φ , subject to certain smoothness assumptions, by outlining the necessary conditions for optimality. Once a good approximation of the value function Φ is computed, this framework can be applied to any initial data and parameters, also allowing for adaptability to perturbations in the system.

4.2. Function Value Approximation. In principle, one could employ any high-dimensional function approximator to parameterize the value function. Yet, due to the universal approximation properties inherent in NNs, we opt for using an NN to parameterize the value function. Designing an effective neural network architecture is essential for various learning

tasks, and it remains an active area of research. In our approach, we treat this as a modular component, providing flexibility. Our framework can seamlessly integrate with any scalar-valued neural network that accepts inputs in \mathbb{R}^{d+1} and possesses at least one continuous derivatives concerning its first $d + 1$ inputs, to allow computations of $\nabla\Phi$.

In our experiments, we use a residual neural network given by

$$(4.4) \quad \Phi_{\theta}(\mathbf{h}_0) = \mathbf{w}^{\top} \text{NN}(\mathbf{h}_0; \theta_{\text{NN}}),$$

with trainable weights θ containing $\mathbf{w} \in \mathbb{R}^m$ and $\theta_{\text{NN}} \in \mathbb{R}^p$. Here the inputs $\mathbf{h}_0 = (t, \mathbf{z}(t); \mathbf{y}) \in \mathbb{R}^{d+1}$ correspond to time-space, and $\text{NN}(\mathbf{h}_0; \theta_{\text{NN}}): \mathbb{R}^{d+1} \rightarrow \mathbb{R}^m$ is a residual neural network (ResNet) [11]

$$(4.5) \quad \begin{aligned} \mathbf{h}_1 &= \sigma(\mathbf{K}_0 \mathbf{h}_0 + \mathbf{b}_0) \\ \mathbf{h}_{i+2} &= \mathbf{h}_{i+1} + \sigma(\mathbf{K}_{i+1} \mathbf{h}_{i+1} + \mathbf{b}_{i+1}), \quad 0 \leq i \leq M-2 \\ \text{NN}(\mathbf{h}_0; \theta_{\text{NN}}) &= \mathbf{h}_M + \sigma(\mathbf{K}_M \mathbf{h}_M + \mathbf{b}_M), \end{aligned}$$

with neural network weights $\theta_{\text{NN}} = (\mathbf{K}_0, \dots, \mathbf{K}_M, \mathbf{b}_0, \dots, \mathbf{b}_M)$ where $\mathbf{b}_i \in \mathbb{R}^m \forall i$, $\mathbf{K}_0 \in \mathbb{R}^{m \times (d+1)}$, and $\{\mathbf{K}_1, \dots, \mathbf{K}_M\} \in \mathbb{R}^{m \times m}$ with M being the depth of the network. We use the element-wise nonlinearity $\sigma(x) = \log(\exp(x) + \exp(-x))$, which is the antiderivative of the hyperbolic tangent, i.e., $\sigma'(x) = \tanh(x)$. For the experiments, we use $m = 64$ nodes per layer and a network depth of $M = 4$.

4.3. Numerical Implementation. We tackle the control problem eq. (4.1) using the discretize-then-optimize approach. We begin by discretizing the constraints and then optimize. To do so, we first sample parameters $\mathbf{y} \sim \eta$ and then use a time discretization of $N + 1$ equidistant time points $t = s_0, \dots, s_N$ with step size $\Delta s = (T - t)/N$ to eliminate the constraints in eq. (2.1b). The specific discretization details for each experiment vary and are discussed in their respective sections. This yields a state trajectory starting at $\mathbf{z}_0 = \mathbf{x}$ via

$$(4.6) \quad \mathbf{z}_{i+1} = \mathbf{z}_i + f(s_i, \mathbf{z}_{i+1}; \mathbf{y}) \Delta s + g(s_i, \mathbf{z}_{i+1}; \mathbf{y}) \mathbf{u}_i \Delta s, \quad i = 0, \dots, N-1,$$

where $\mathbf{z}_i = \mathbf{z}(s_i)$ and $\mathbf{u}_i = \mathbf{u}^*(s_i, \mathbf{z}_i, \nabla_{\mathbf{z}} \Phi_{\theta}(s_i, \mathbf{z}_i; \mathbf{y}))$ is the optimal control obtained from the feedback form, that is, from eq. (4.3), computed by equating $\nabla_{\mathbf{u}} \mathcal{H} = 0$. Finally, we approximate the objective functional via

$$(4.7) \quad J(s_k, \mathbf{z}, \mathbf{u}; \mathbf{y}) = \Delta s \sum_{i=k}^N L(s_i, \mathbf{z}_i, \mathbf{u}_i) + G(\mathbf{z}_N),$$

and simultaneously, the penalty term $P_{\text{HJB}, \mathbf{y}}$ in a similar manner.

In principle, any stochastic approximation approach can be used to solve the above optimization problem. Here, we use Adam [17] and sample a minibatch of trajectories originating in i.i.d. samples from η with an initial learning rate of 0.075. During training, the learning rate gradually diminishes with an exponential decay rate of 0.975 until it stabilizes at 0.0025. For each training iteration, we randomly select a batch of 20 problem parameters from the distribution η . Following the HJB framework, we evaluate controls for each problem and evolve the systems accordingly. Subsequently, we compute the losses, utilizing them to update the network weights, as illustrated in Algorithm 1.

Algorithm 1 Model-based training approach

Require: Number of training problems P , problem parameter distribution η , initial network weights θ , Hamiltonian H , and loss weighting factors $(\beta_1, \beta_2, \beta_3)$

-
- 1: **Initial Setup for Training**
 - 2: *Derive Feedback Form Expression*
 - 3: Feedback_Form : $(-\nabla_{\mathbf{z}}\Phi_{\theta}, f, g) \mapsto \mathbf{u}$
 - 4:
 - 5: *Assemble Randomized Problems*
 - 6: Sample P parameters $\{\mathbf{y}_i\}_{i=1}^P \sim \eta$
 - 7: Store **matrices** for f and g corresponding to $\{\mathbf{y}_i\}_{i=1}^P$
 - 8:
 - 9: **HJB Training Iteration**
 - 10: *Sample Batch of Problems*
 - 11: Retrieve **matrices** for \mathbf{y}_p with $p \sim \text{Uniform}(\{1, \dots, P\})$
 - 12:
 - 13: *Assess HJB Control Performance*
 - 14: Set $s_0 = 0$, $\mathbf{z}_0 = \mathbf{x}$, $J = 0$, and $P_{\text{HJB}, \mathbf{y}_p} = 0$
 - 15: **while** $i \leq N$ **do**
 - 16: *Derive Control from Feedback Form*
 - 17: Evaluate network $\Phi_{\theta}(s_i, \mathbf{z}_i, \mathbf{y}_p)$ and gradient $\nabla_{\mathbf{z}}\Phi_{\theta}(s_i, \mathbf{z}_i; \mathbf{y}_p)$
 - 18: $\mathbf{u}_i = \text{Feedback_Form}(-\nabla_{\mathbf{z}}\Phi_{\theta}(s_i, \mathbf{z}_i; \mathbf{y}_p), f, g)$
 - 19:
 - 20: *Evolve Systems in Time*
 - 21: $\mathbf{z}_{i+1} \leftarrow \text{Time_Integrator}(\mathbf{z}_i, \mathbf{u}_i; \mathbf{y}_p)$
 - 22: $s_{i+1} \leftarrow s_i + \Delta s$
 - 23:
 - 24: *Update Intermediate Losses*
 - 25: $J \leftarrow J + L(s_i, \mathbf{z}_i, \mathbf{u}_i)\Delta s$
 - 26: $P_{\text{HJB}, \mathbf{y}_p} \leftarrow P_{\text{HJB}, \mathbf{y}_p} + \beta_1 |H(s_i, \mathbf{z}_i, \nabla_{\mathbf{z}}\Phi_{\theta}(s_i, \mathbf{z}_i; \mathbf{y}_p); \mathbf{y}_p) - \partial_s \Phi_{\theta}(s_i, \mathbf{z}_i, \mathbf{y}_p)|\Delta s$
 - 27: **end while**
 - 28: $J \leftarrow J + G(\mathbf{z}_N)$
 - 29: $P_{\text{HJB}, \mathbf{y}_p} \leftarrow P_{\text{HJB}, \mathbf{y}_p} + \beta_2 |G(\mathbf{z}_N - \Phi_{\theta}(s_N, \mathbf{z}_N, \mathbf{y}_p))| + \beta_3 |\nabla_{\mathbf{z}}G(\mathbf{z}_N) - \nabla_{\mathbf{z}}\Phi_{\theta}(s_N, \mathbf{z}_N, \mathbf{y}_p)|$
 - 30:
 - 31: *Update Networks Weights*
 - 32: $\theta \leftarrow \text{Optimizer}(J + P_{\text{HJB}, \mathbf{y}_p})$
-

5. DATA-DRIVEN APPROACH

We briefly review the data-driven approach, in particular, the Reinforcement Learning (RL) framework, with an emphasis on Actor-Critic algorithm used to approximate the optimal policy in our work; our presentation follows [5, 33].

Reinforcement learning (RL) provides a general framework for approximating policies through a series of interactions with an environment. More precisely, an RL environment specifies all possible system states, a description of admissible actions, along with a model governing the evolution of the system space when an action is performed. In RL language,

the controls are referred to as the actions. The environment is paramount for RL algorithms, and its proper definition is crucial.

Let π_{θ_a} denotes the policy, parameterized by parameters θ_a , which is a mapping from the state space to the action space. The policy can be either deterministic, denoted as $\mathbf{u}_i = \pi_{\theta_a}(\mathbf{z}_i)$, or stochastic, indicated as $\mathbf{u}_i \sim \pi_{\theta_a}(\cdot|\mathbf{z}_i)$. Using eq. (4.6), a policy generates a sequence of states and actions, $(\mathbf{z}_i, \mathbf{u}_i)_{i=0}^N$, referred to as an episode.

In order to evaluate the performance of a policy, it is necessary to create functions `step()` and `reset()` governing the problem dynamics and the interaction between the agent and the environment. Aiming to address the optimization problem introduced in section 2, these functions operate as follows

- `reset()`: This function initializes or resets the environment to its initial state, \mathbf{z}_0 , preparing it for the new episode.
- `step()`: Given an action \mathbf{u}_i as input, determined by a policy, it returns the following:
 - The next state \mathbf{z}_{i+1} using the dynamics described in eq. (4.6).
 - A scalar feedback signal representing the objective function, known as the reward,

$$r_i = \begin{cases} \Delta s L(s_i, \mathbf{z}_i, \mathbf{u}_i), & i < N \\ \Delta s L(s_N, \mathbf{z}_N, \mathbf{u}_N) + G(\mathbf{z}_N), & i = N \end{cases}.$$

- The termination status indicates the terminal time T has been reached or the current episode has terminated.

Specific environment details for the problems considered are provided in section 6.

The goal is to identify an optimal policy in order to minimize the cumulative reward, called return¹, given by the value function

$$(5.1) \quad \Psi(\theta_a) = \mathbb{E}_{\pi_{\theta_a}, \mathbf{y} \sim \eta} \left\{ \sum_{i=0}^N r_i \right\} = \mathbb{E}_{\pi_{\theta_a}, \mathbf{y} \sim \eta} \{ J(s_0, \mathbf{z}, \mathbf{u}; \mathbf{y}) \}.$$

When the policy is deterministic, the expectation over π_{θ_a} in eq. (5.1) is omitted, making the return equivalent to the one in the neural-HJB training defined in eq. (4.7).

Remark 5.1. When starting from the initial state \mathbf{z}_0 and following the optimal policy $\pi_{\theta_a}^*$, we recover the original value function Φ in eq. (2.2).

In our work, we consider the policy to be stochastic as they provide additional flexibility, robustness, and adaptability that can be advantageous in complex and uncertain environments.

Now that we have established a loss function representative of the original optimization problem, we must also review the expression for the gradients with respect to θ_a for updating these parameters. This expression is provided by the following foundational result from the theory of RL.

Theorem 5.2. [33, Policy Gradient Theorem, Chapter 13] *The gradient of the cumulative reward objective function eq. (5.1) can be expressed in terms of the policy gradients as follows:*

$$(5.2) \quad \nabla_{\theta_a} \Psi(\theta_a) = \mathbb{E}_{\pi_{\theta_a}, \mathbf{y} \sim \eta} \left\{ \sum_{i=0}^N \nabla_{\theta_a} \log \pi_{\theta_a}(\mathbf{u}_i|\mathbf{z}_i) J(s_i, \mathbf{z}, \mathbf{u}; \mathbf{y}) \right\}.$$

¹Conventional RL literature assumes that the objective function is being maximized; for the purposes of aligning with the optimal control problem setup from previous sections, we instead aim to minimize the loss (which can be interpreted as the negative reward in standard RL literature).

While the direct use of Theorem 5.2 for policy optimization can work effectively in some cases, the practical performance often suffers from high variance in the gradient estimate, and thus produce slow learning. To reduce variance effects and increase stability, many policy-based RL algorithms subtract the cumulative reward by a baseline, $b(\mathbf{s})$:

$$(5.3) \quad \nabla_{\theta_a} \Psi(\theta_a) = \mathbb{E}_{\pi_{\theta_a}, \mathbf{y} \sim \eta} \left\{ \sum_{i=0}^N (J(s_i, \mathbf{z}_i, \mathbf{u}_i; \mathbf{y}) - b(\mathbf{z}_i)) \nabla_{\theta_a} \log \pi_{\theta_a}(\mathbf{u}_i | \mathbf{z}_i) \right\}.$$

Intuitively, making the cumulative reward smaller by subtracting it with a baseline will make smaller gradients, and thus smaller and more stable updates.

5.1. Actor-Critic Models. Selecting an effective baseline poses a challenge, but the state-value function is a suitable choice, making both the value function and policy learnable. This creates a two-component RL framework known as an actor-critic model:

- The actor π_{θ_a} determines actions based on the current state (i.e. defines the policy).
- The critic Ψ_{θ_c} , parameterizing the baseline with parameters θ_c , assesses the approximate value of the current state (i.e. provides value function estimates).

and both are parameterized by neural networks.

Now that the value function is also made learnable, that means we must provide an objective for the critic network to learn the parameters θ_c . Since the role of the critic is to provide a baseline estimate for the return, a natural choice for this objective is the expected value of the squared error:

$$(5.4) \quad P_{\text{critic}}(\theta_c) = \sum_{i=0}^N |\Psi_{\theta_c}(\mathbf{z}_i) - J(s_i, \mathbf{z}, \mathbf{u}; \mathbf{y})|^2.$$

In summary, for the actor-critic models, we are approximately solving the minimization problem given by

$$\min_{\theta_a, \theta_c} \mathbb{E}_{\pi_{\theta_a}, \mathbf{y} \sim \eta} \{J(s_0, \mathbf{z}, \mathbf{u}; \mathbf{y}) + \beta_5 P_{\text{critic}}(\theta_c)\},$$

where $\beta_5 \in \mathbb{R}_+$ controls the relative contribution of critic. Although there are several actor-critic algorithms available, in this work we use two prominent, state-of-the-art algorithms: Proximal Policy Optimization (PPO) and Twin Delayed Deep Deterministic Policy Gradients (TD3). Both PPO and TD3 are advanced versions of the actor-critic framework discussed above, each addressing critical aspects stability, mitigating overestimation bias, or providing better exploration strategies. For in-depth explanations and implementation specifics, we direct readers to [29, 10].

5.2. RL Network Architecture. Since the observation data for our experiments is spatially structured on a two-dimensional grid, we employ convolutional network architectures to process the system state at each time-step. Both the actor and critic networks share the same network architecture with the exception of the final layer which is adapted to the specific format of the actions and value outputs, respectively. As illustrated in Figure 1, the networks consist of three convolutional layers with 3×3 kernels each followed by 2×2 max-pooling layers; the series of convolutional layers is then followed by two dense layers and a final linear layer is used to produce the position/variance in the case of the actor network and the value prediction in the case of the critic network. All layers are equipped with hyperbolic tangent activation functions, and orthogonal initialization is used for both the convolutional and dense weights.

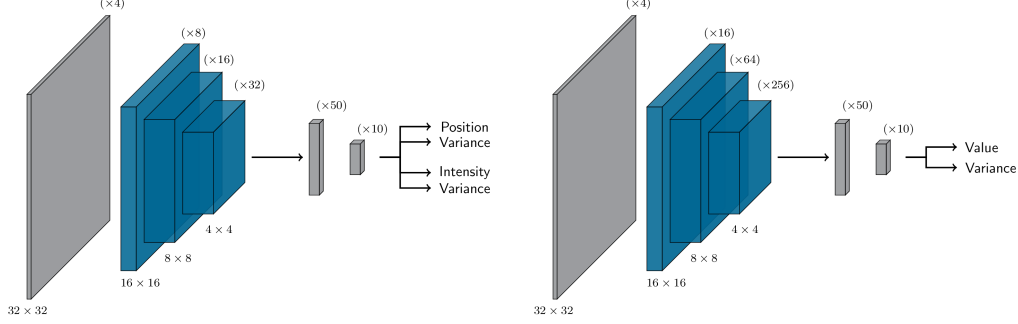


FIGURE 1. Network architectures for the actor (left) and critic (right) components of the RL models. Both networks receive input arrays containing the values of $\mathbf{z}(s)$, \mathbf{y} , and s . Convolutional and max-pooling layers (blue) process the data received from the PDE environment to extract features. These features are then flattened and passed to dense layers (grey) to form the position, variance, and value predictions.

We train the networks using a pair of Adam optimizers, one used for the actor network and the other used for the critic, and apply an exponential decay to the learning rates which are both initially set to 10^{-4} . The observation states are also normalized using an exponential moving average estimate for the mean and variance of the input data in each batch.

It is essential to highlight the difference in network architectures employed for the OC and RL approaches. The OC approach necessitates an architecture with at least one continuous derivative with respect to the network inputs. In contrast, the RL approach only requires policies that are differentiable with respect to the network weights. Because of this, RL is compatible with most off-the-shelf architectures, while architecture choices for the OC approach are slightly more restricted.

6. NUMERICAL RESULTS

In this section we compare the model-based and data-driven training approaches for a control problem involving the advection diffusion equation. Since the ground-truth solutions for these problems are not available, we use conventional, gradient-based solutions as baselines to approximate the optimal solutions for fixed parameters in a test set. All models were trained using 10 cores of an Intel Xeon Platinum 8176 CPU at 2.10GHz.

In our initial experiments, we trained all models using the same network architecture; however, we found the OC and RL approaches required distinct design choices to attain the best results. When using a convolutional architecture for the OC training procedure, the gradient signals appeared to be too weak, and models failed to train from the start. For the RL models, replacing convolutional layers with a residual network led to a noticeable drop in performance that remained after several iterations of hyperparameter tuning. To provide a fair assessment, we present numerical results using the architecture that yields the best performance for each approach.

6.1. Advection-Diffusion Problem Formulation. For our numerical tests, we consider the solution $a(\cdot, \cdot)$ to an advection-diffusion PDE defined on a square domain $\Omega = [0, 1] \times [0, 1] \subset \mathbb{R}^2$ as part of the system state \mathbf{z} . The control problem is based on a two-dimensional,

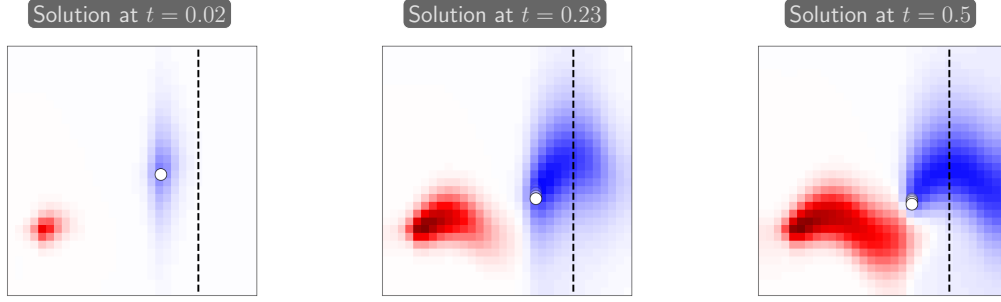


FIGURE 2. Example evolution of advection diffusion system

continuous control vector $\mathbf{u}(s) = [u_1(s), u_2(s)]^\top$, aiming to prevent positive values of the solution $a(\cdot, \cdot)$ from occurring in a target region $\Omega_{\text{targ}} = \{(x_1, x_2) \in \Omega : x_1 > 0.75\}$ at the final time $T = 0.75$. A motivating contaminant control example is illustrated in Figure 2 where a represents contaminant concentration (in red) originating from a source location corresponding to fixed \mathbf{y} . The parameters \mathbf{y} either contains information about the source location (Experiment 1) or both the source location and phase of advecting velocity (Experiment 2). The goal is to prevent this contamination from reaching the target subdomain Ω_{targ} which is shown to the right of the vertical dashed line. To achieve this, an optimal sequence of locations and magnitudes for the sink (in blue) must be found, both of which will depend strongly on the parameter \mathbf{y} under consideration.

For a given $\mathbf{y} \in \eta$, the objective function for the problem is given explicitly by:

$$(6.1) \quad \frac{1}{2} \int_0^T |\mathbf{u}(s)|^2 ds + \rho \int_{\Omega_{\text{targ}}} |\max\{a(T, (x_1, x_2)), 0\}| dx_1 dx_2$$

and part of the dynamics from eq. (2.1b) are prescribed by an advection-diffusion PDE of the form

$$(6.2) \quad \partial_s a + \text{div}(\kappa \nabla a) + \varepsilon_{\mathbf{y}} \nabla a + \varphi_{\mathbf{y}} = u_1 Q(\alpha)$$

with initial condition $a(0, x_1, x_2) = 0$ and homogeneous Neumann boundary conditions.

The controls \mathbf{u} influence system dynamics through the sink term ‘ Q ’. Here, u_1 determines the magnitude of the sink while u_2 controls the sink’s velocity via the location variable α by:

$$\alpha(t) = \alpha(0) + \int_0^t u_2(s) ds \quad \text{with} \quad \alpha(0) = 0.5.$$

For the sink term Q , we consider

$$Q(x_1, x_2, \alpha(t)) = 25 \cdot \exp(|x_1 - 0.6|/0.025 + |x_2 - \alpha(t)|/0.15).$$

Each parameter $\mathbf{y} \in \eta$ consists of three components $\mathbf{y} = [\mathbf{y}_{x_1}, \mathbf{y}_{x_2}, \mathbf{y}_v]$. The parameters \mathbf{y}_{x_1} and \mathbf{y}_{x_2} denote the x_1 and x_2 coordinates of the location of the source term, $\varphi_{\mathbf{y}}$, given by

$$(6.3) \quad \varphi_{\mathbf{y}}(x_1, x_2) = (c/\sigma_s) \exp(-(|x_1 - \mathbf{y}_{x_1}| + |x_2 - \mathbf{y}_{x_2}|)/\sigma_s)$$

while \mathbf{y}_v adjusts the phase of the velocity field, $\varepsilon_{\mathbf{y}}$.

For our first family of problems, we consider a fixed velocity field, but randomized source locations, in a horizontal setup with parameters

$$\varepsilon_{\mathbf{y}}(x_1, x_2) = [25, 0], \quad c = 5, \quad \sigma_s = 0.01, \quad \text{and} \quad \kappa = 0.008.$$

We then consider a relatively challenging family of problems, sinusoidal setup, which incorporates a more complex velocity field and extends problem randomization to control the phase of the velocity as well:

$$(6.4) \quad \varepsilon_{\mathbf{y}}(x_1, x_2) = \begin{bmatrix} (1 + x_1) \cdot \sqrt{0.9^2 - (0.75 \cdot \cos(1.1 - x_1) \cdot \sin(4\pi(x_1 - \mathbf{y}_v)))^2} \\ -0.9 \cdot \cos(1.1 - x_1) \cdot \sin(4\pi(x_1 - \mathbf{y}_v)) \end{bmatrix}$$

For the sinusoidal setup, we also adjust the source magnitude to $c = 0.5$ and the source size to $\sigma_s = 0.025$ to produce more natural flows for the modified velocity field.

We sample the components of \mathbf{y} from the uniform distributions

$$\mathbf{y}_{x_1} \sim \text{Unif}(0.1, 0.25) \quad , \quad \mathbf{y}_{x_2} \sim \text{Unif}(0.2, 0.8) \quad , \quad \mathbf{y}_v \sim \text{Unif}(-0.425, 0.0)$$

so that the source locations are varied in the horizontal and vertical directions across the left side of the domain. For the sinusoidal setup, the velocity field directs concentration near the source upward for values of $\mathbf{y}_v \approx -0.425$ and directs downward for $\mathbf{y}_v \approx 0.0$.

Finally, to balance the importance of the running cost and terminal cost terms in the objective function, we choose a scaling factor of $\rho = 40$ in eq. (6.1). This is generally necessary since the scale of the action space does not always match that of the state space, and one of the loss components can dominate the other if left unweighted.

6.1.1. Discretization. Since the continuous formulation results in an infinite dimensional optimal control problem, we cannot apply numerical methods to the problem described above directly. Instead we consider an approximate formulation arising from the spatial discretization of eq. (6.2) using finite elements.

Denoting the discretized, FEM representation of $a(s, x_1, x_2)$ by $\mathbf{a}(s)$, the state vector for the problem is given by:

$$\mathbf{z}(s) = [\mathbf{a}(s), \alpha(s)]^\top.$$

The dynamics for the \mathbf{a} component of the state vector are defined by the linear systems associated with the FEM formulation of eq. (6.2). By construction, the state dynamics for α are simply $d_s \alpha(s) = u_2(s)$.

For the spatial discretization, we have selected linear, triangular elements with nodes associated with a uniform 32×32 grid. The FEM representation for the concentration \mathbf{a} is passed to the neural networks by evaluating pointwise on the grid locations $\{(x_1^i, x_2^j)\}_{i,j=1}^{32}$ with $x_1^i = i \cdot \Delta x_1$, $x_2^j = j \cdot \Delta x_2$, and $\Delta x_1 = \Delta x_2 = 1/31$. We further discretize the PDE in time via implicit Euler with a step count of $N = 25$ and step size $\Delta t = 0.02$ to obtain the fully discretized control objective

$$(6.5) \quad J(0, \mathbf{z}, \mathbf{u}; \mathbf{y}) := \frac{1}{2} \sum_{i=0}^{25} |\mathbf{u}_i|^2 \Delta t + \rho \sum_{i,j=1}^{32} 1_{\Omega_{\text{targ}}}(x_1^i, x_2^j) |\max\{\mathbf{a}(T), 0\}| \Delta x_1 \Delta x_2.$$

6.1.2. Feedback Form for HJB. To apply the proposed model-based approach procedure, we first need to derive the feedback form for the optimal control. This expression depends on the specific PDE under consideration and provides a natural way of incorporating system knowledge into the training procedure. As stated in eq. (2.5), the optimal control is a maximizer for the Hamiltonian evaluated at $\nabla_{\mathbf{z}} \Phi$. By taking the gradient of the Hamiltonian

and setting the resulting expression to zero, the feedback form for both problem setups is given by:

$$\mathbf{u}(s) = \left[-\mathbf{Q}^T \nabla_{\mathbf{a}} \Phi(s), -\nabla_{\alpha} \Phi(s, \mathbf{z}(s); \mathbf{y}) \right]^T$$

where \mathbf{Q} is the finite element matrix associated with the sink term ‘ Q ’ in eq. (6.2).

6.1.3. Parallel Implementation of RL environments. The FEM calculations used to simulate the PDE environment present a significant computational bottleneck in the training procedure. Fortunately, both the PPO and TD3 algorithms can be trained using interactions with multiple, distinct environments in parallel. This is possible since both algorithms decouple the actor weights used during optimization from the network weights used in the simulations². In particular, since both algorithms update policy weights based on interactions performed by decoupled policies, it is possible to run multiple episodes in parallel before calculating losses and applying gradient updates. To take advantage of this, we employ OpenMPI and MPI for Python to parallelize the interactions of the actor network with several different environment realizations simultaneously. The environments are initialized in parallel, observation data is gathered to the root node and passed to the actor/critic networks as a single batch, and the proposed actions are then broadcast back to the respective environments. We repeat this process until all environments have completed a full episode. After all episodes are complete, we compute the associated returns, group transitions from all environments into minibatches, and perform gradient updates.

6.2. Hyperparameter Selection. Determining hyperparameters, including network architectures and optimization parameters, plays a crucial role in neural network methodologies. In our observation, the selection of hyperparameters frequently depends on the specific approach and problem at hand. Developing well-founded mathematical principles for parameter selection in these models represents a significant area for future research, but it exceeds the scope of this paper. Nonetheless, we provide our insights into hyperparameter selection for the two approaches outlined in this paper.

The proposed HJB approach requires tuning for only a small handful of parameters: the networks’ width and depth, the learning rate and decay schedule, the batch size, and three weights ($\beta_1, \beta_2, \beta_3$) which determine how much the HJB constraints contribute to the loss. The RL models considered in this work have a much larger set of hyperparameters and require a substantial number of system solves to identify the correct training settings. This is particularly true of scaling and clipping parameters that are used to prevent the RL training procedure from becoming unstable. When these parameters are not set correctly, the models’ performance will often deteriorate midway through training, and the procedure must be restarted.

6.3. Baseline via Gradient-Based Solutions. To understand how the proposed, amortized procedure compares with more conventional approaches, we now review how gradient-based methods handle this class of control problems. These methods apply to a single problem realization (i.e., fixed value of \mathbf{y}) and rely on gradient information, namely $\nabla_{\mathbf{u}} J$, to identify an optimal control. For this work, we have implemented a gradient-based solver using FEM matrices extracted from FEniCS and automatic differentiation provided by PyTorch to retrieve the necessary gradients. We then use the limited memory Broyden-Fletcher-Goldfarb-Shanno algorithm to search the control space for an optimal solution. We use the

²PPO decouples weights through an ‘old’ policy, and TD3 uses a related technique using a ‘target’ policy.

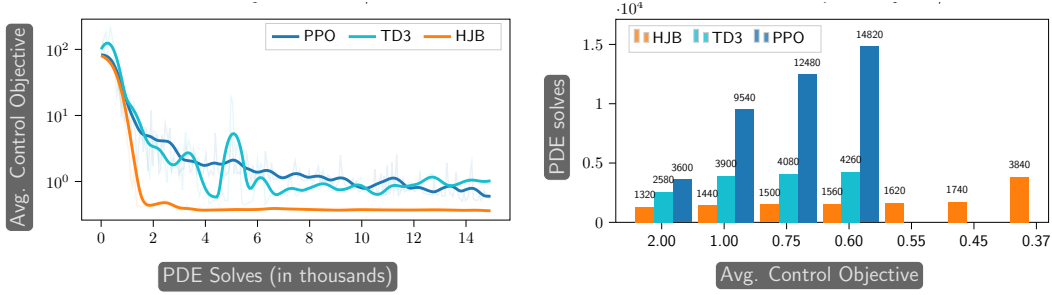


FIGURE 3. Horizontal problem setup: (left) Validation loss during training and (right) number of PDE solves required for different target accuracies of control objective.

solutions obtained from this gradient-based search as proxies for the true optimal solutions (which are intractable for the problems considered in this work).

Here, it is important to note that the control obtained from the gradient-based method is specific to the given parameter. While the control may perform well for nearby parameters, in general, changes in the parameter require another solve. In many cases, the original control does not even provide an effective initialization point for new problems (since the optimal control can change considerably when system dynamics are modified). Because of this, the initialization procedure is another important and non-trivial aspect of gradient-based methods. Even though these methods are designed to solve a single problem, unlike amortized approaches that target a number of problems at once, the gradient-based search can fail to converge to an optimal control without proper initialization.

6.4. Assessment of HJB and RL Performance. For the first set of experiments, we consider the horizontal velocity setup with two controls corresponding to the magnitude and velocity of the sink term. The RL and HJB models are tasked with positioning the sink in locations that block the concentration from entering the target region while using as little movement as possible. To evaluate each model’s performance, we assess the accuracy of the models on a set of fixed validation problems throughout training. For the validation set, we have selected parameter values $\mathbf{y}_{x_1} \in \{0.125, 0.225\}$ and $\mathbf{y}_{x_2} \in \{0.25, 0.4, 0.5, 0.6, 0.75\}$. This corresponds to 10 realizations of the horizontal setup with source locations spread across the left side of the domain. The results of this experiment are summarized in Figure 3 where we observe that the HJB framework yields several, noticeable improvements over both RL models.

The most clear, and practically significant, distinction between the HJB and RL training procedures is the rapid drop in the HJB validation loss at the very start of training. This is perhaps to be expected thanks to the gradient information exposed by the HJB training formulation, while the RL models are initially reliant on an uninformed, trial-and-error state of exploration. For practical applications, this is a key feature of the HJB training procedure; the model is able to identify effective control policies using far fewer forward-model PDE solves than its RL counterparts. By relying on fewer forward solves, the HJB approach has the potential to be applied to more computationally expensive simulations where performing the tens of thousands of queries required by RL models is simply impractical.

To assess how well the model-based approach framework extends to more complicated systems, we now turn to evaluating its performance on the sinusoidal setup. This setup

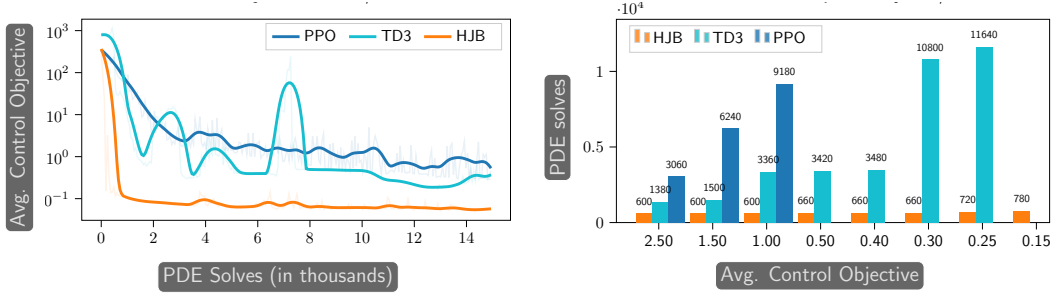


FIGURE 4. Sinusoidal problem setup: (left) Validation loss during training and (right) number of PDE solves required for different target accuracies of control objective.

introduces more complex system dynamics which incorporate non-uniform velocity fields for advection. We also add another layer of randomization by varying the phase of the velocity field according to an additional problem parameter \mathbf{y}_v . These variations in the velocity field are designed to reflect uncertain ambient conditions (such as weather) which may need to be taken into account when developing control strategies for practical applications. This form of randomization influences how systems evolve in time and will help us gauge how well the model-based approach and RL approaches are able to amortize over problems with substantially different dynamics.

For the sinusoidal setup, we define the validation set using parameter values selected from $\mathbf{y}_{x_1} \in \{0.125, 0.225\}$, $\mathbf{y}_{x_2} \in \{0.25, 0.4, 0.5, 0.6, 0.75\}$, and $\mathbf{y}_v \in \{-0.35, -0.2125, -0.1\}$. This yields 30 problem realizations with source locations spread across the left side of the domain and velocity fields which direct concentration near these source terms upward, horizontally, as well as downward.

The results for the sinusoidal setup are depicted in Figure 4, where we once again observe a clear advantage in data efficiency for the HJB model. The HJB model achieves an average control objective of 0.15 using only 780 PDE solves. However, both RL models fail to achieve an average control objective below 0.25 even with the full 15,000 solves.

In Figure 5, we also present the suboptimality of HJB and RL approaches compared to the baseline, as discussed in Section 6.3. It can be observed that the HJB model achieves much lower suboptimality than RL models with significantly fewer PDE solves. This difference is particularly pronounced in the sinusoidal setup, where the HJB approach can achieve a suboptimality of 0.03 in 4740 PDE solves, while RL approaches fail to go below 0.20.

This faster convergence can be partially attributed to the training algorithms used in RL. While both RL models succeed in preventing positive concentrations from reaching the target region, they do so with unnecessary movement. The RL policies often exhibit bias in initial movement in one direction (e.g., drifting downward at the start of a simulation) and then correct with a sharp reversal in direction if needed. These inefficiencies result in much larger running costs for the RL models and prevent them from reaching the control objective levels attained by the HJB approach.

7. DISCUSSION

We consider deterministic, finite-time optimal control problems with unknown or uncertain parameters and aim to approximate optimal policies for all parameters with neural

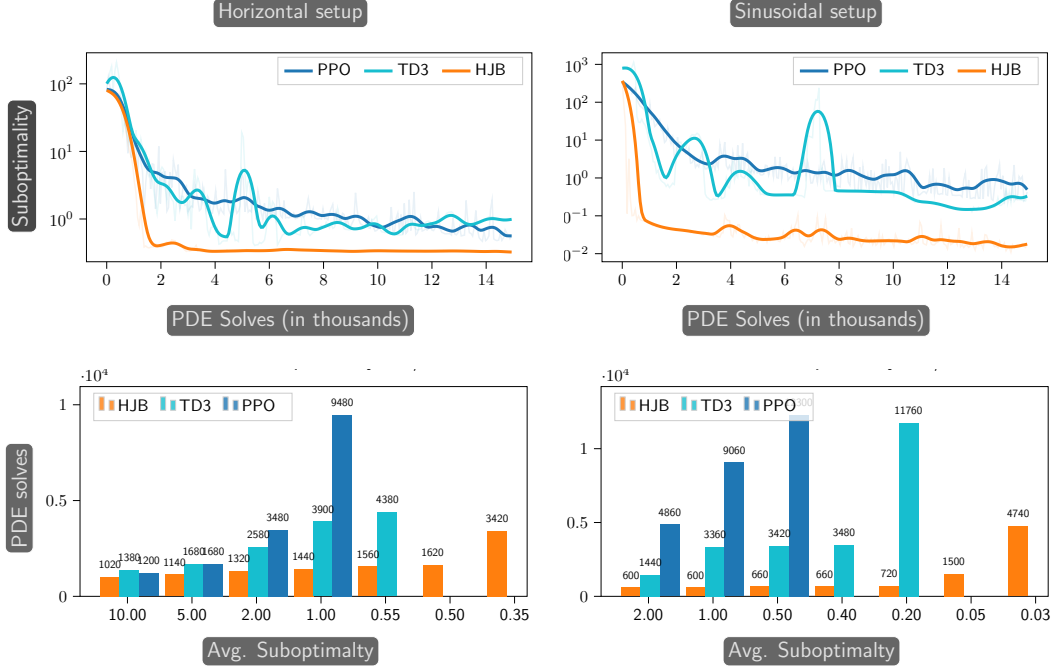


FIGURE 5. Suboptimality, relative to the baseline, on validation problems for the horizontal (left column) and sinusoidal (right column) problem setups.

networks. We compare to training paradises. On the one hand, our model-based approach parameterizes the value function using a neural network and derives the policy from the feedback form. By leveraging control theory, this approach incorporates the system’s physics by penalizing the Hamilton-Jacobi-Bellman equation satisfied by the value function during training. On the other hand, the data-driven approach adopts state-of-the-art actor-critic RL frameworks and trains separate networks for the policy (actor) and the value function (critic). Both networks are trained exclusively from observational data. Despite drawing inspiration from control theory, particularly Dynamic Programming, both approaches exhibit distinct behaviors in practical applications.

Although we strived to use almost identical learning problems in both paradigms, we had to allow for some differences to account for their assumptions. Most importantly, our model-based approach had to use a simpler network architecture to ensure the differentiability with respect to the inputs needed to apply the feedback form. While non-differentiable off-the-shelf CNN architectures worked well for the data-driven approach, the training did not yield adequate results using the simpler architecture.

We apply both approaches to a model problem inspired by contaminant containment to assess accuracy and efficiency. In this scenario, the state of the system is governed by a two-dimensional advection-diffusion partial differential equation (PDE), and the objective is to prevent the contaminant from reaching a target region by controlling the location and intensity of a sink, with the parameter reflecting various scenarios for the source locations and velocity fields.

While both approaches follow an unsupervised training regime, our numerical results reveal that the model-based approach approximates a reasonable policy with much lower sub-optimality, when compared to a gradient-based baseline. Notably, it achieves this with far fewer PDE solves than RL (see Figure 5). The superior performance of the model-based approach can be attributed to the incorporation of physics and system derivatives guided by control theory. In contrast, lacking awareness of this information, RL demands a larger number of PDE solutions. During RL training, many models showed promising learning for several thousand PDE solves but eventually diverged and were unable to recover. This phenomenon never occurred in the model-based approach.

Despite RL’s data-prohibitive nature, its non-intrusive and gradient-free characteristics make it widely applicable and suitable for experimenting with new problems lacking well-defined models or facing challenges in efficiently computing feedback forms and system derivatives. As part of future work, we aim to extend our model-based approach to such scenarios and revisit the comparison against RL.

Another advantage of the model-based approach lies in its simpler hyperparameter setup, requiring fewer than half the number of hyperparameters compared to RL approaches. Effective hyperparameters identified for one problem setup could be seamlessly applied to other problems without modification. Conversely, RL training procedures proved sensitive to hyperparameter choices, often necessitating re-tuning between problems for convergence. This again emphasizes the data efficiency of the model-based approach.

As a part of future work, we plan to compare the methods for more complex problems and investigate their scalability using increasingly finer discretizations.

ACKNOWLEDGMENTS

LR’s and DV’s work was supported in part by NSF awards DMS 1751636 and DMS 2038118, AFOSR grant FA9550-20-1-0372, and US DOE Office of Advanced Scientific Computing Research Field Work Proposal 20-023231. NW’s and BV’s work was supported in part by Sandia National Laboratories which is a multimission laboratory managed and operated by National Technology and Engineering Solutions of Sandia LLC, a wholly owned subsidiary of Honeywell International, Inc., for the U.S. Department of Energy’s National Nuclear Security Administration under Contract DE-NA0003525, and US Department of Energy, and Office of Advanced Scientific Computing Research, Field Work Proposal 20-023231.

REFERENCES

- [1] Susan Amin, Maziar Gomrokchi, Harsh Satija, Herke van Hoof, and Doina Precup. A survey of exploration methods in reinforcement learning. *arXiv preprint arXiv:2109.00157*, 2021.
- [2] Francesco Ballarin, Elena Faggiano, Andrea Manzoni, Alfio Maria Quarteroni, Gianluigi Rozza, Sonia Ippolito, Carlo Antona, and Roberto Scrofani. Numerical modeling of hemodynamics scenarios of patient-specific coronary artery bypass grafts. *Biomechanics and Modeling in Mechanobiology*, 16:1373–1399, 2017.
- [3] Somil Bansal and Claire J. Tomlin. DeepReach: A deep learning approach to high-dimensional reachability. In *IEEE International Conference on Robotics and Automation (ICRA)*, pages 1817–1824, 2021.
- [4] Christopher Berner, Greg Brockman, Brooke Chan, Vicki Cheung, Przemyslaw Debiak, Christy Dennison, David Farhi, Quirin Fischer, Shariq Hashme, Christopher Hesse, Rafal Józefowicz, Scott Gray, Catherine Olsson, Jakub W. Pachocki, Michael Petrov, Henrique Pondé de Oliveira Pinto, Jonathan Raiman, Tim Salimans, Jeremy Schlatter, Jonas Schneider, Szymon Sidor, Ilya Sutskever, Jie Tang, Filip Wolski, and Susan Zhang. Dota 2 with large scale deep reinforcement learning. *ArXiv*, abs/1912.06680, 2019.

- [5] Dimitri P. Bertsekas. *Reinforcement learning and optimal control*. Athena Scientific Optimization and Computation Series. Athena Scientific, Belmont, MA, [2019] ©2019. Second printing with editorial revisions.
- [6] Rodrigo C. Carlson, Ioannis Papamichail, Markos Papageorgiou, and Albert Messmer. Optimal motorway traffic flow control involving variable speed limits and ramp metering. *Transportation Science*, 44(2):238–253, 2010.
- [7] Minmin Chen, Alex Beutel, Paul Covington, Sagar Jain, Francois Belletti, and Ed H. Chi. Top-k off-policy correction for a reinforce recommender system. *Proceedings of the Twelfth ACM International Conference on Web Search and Data Mining*, 2018.
- [8] Nicola Demo, Maria Strazzullo, and Gianluigi Rozza. An extended physics informed neural network for preliminary analysis of parametric optimal control problems. *arXiv:2110.13530*, 2021.
- [9] Wendell H. Fleming and H. Mete Soner. *Controlled Markov Processes and Viscosity Solutions*, volume 25 of *Stochastic Modelling and Applied Probability*. Springer, New York, second edition, 2006.
- [10] Scott Fujimoto, Herke van Hoof, and David Meger. Addressing function approximation error in actor-critic methods. In Jennifer Dy and Andreas Krause, editors, *Proceedings of the 35th International Conference on Machine Learning*, volume 80 of *Proceedings of Machine Learning Research*, pages 1587–1596. PMLR, 10–15 Jul 2018.
- [11] Kaiming He, Xiangyu Zhang, Shaoqing Ren, and Jian Sun. Deep residual learning for image recognition. In *Proceedings of the IEEE Conference on Computer Vision and Pattern Recognition (CVPR)*, June 2016.
- [12] Peter Henderson, Riashat Islam, Philip Bachman, Joelle Pineau, Doina Precup, and David Meger. Deep reinforcement learning that matters. In *Proceedings of the AAAI conference on artificial intelligence*, volume 32, 2018.
- [13] Rakhon Hwang, Jae Yong Lee, Jin Young Shin, and Hyung Ju Hwang. Solving PDE-constrained control problems using operator learning. In *Proceedings of the AAAI Conference on Artificial Intelligence*, volume 36, pages 4504–4512, 2022.
- [14] Jemin Hwangbo, Joonho Lee, Alexey Dosovitskiy, Dario Bellicoso, Vassilios Tsounis, Vladlen Koltun, and Marco Hutter. Learning agile and dynamic motor skills for legged robots. *Science Robotics*, 4, 2019.
- [15] Alex Irpan. Deep reinforcement learning doesn’t work yet. 2018.
- [16] Wei Kang, Qi Gong, and Tenavi Nakamura-Zimmerer. Algorithms of data development for deep learning and feedback design. *arXiv:1912.00492*, 2019.
- [17] Diederik P Kingma and Jimmy Ba. Adam: A method for stochastic optimization. *arXiv:1412.6980*, 2014.
- [18] Karl Kunisch and Daniel Walter. Semiglobal optimal feedback stabilization of autonomous systems via deep neural network approximation. *ESAIM: Control, Optimisation and Calculus of Variations*, 27, 2021.
- [19] Karl Kunisch and Daniel Walter. Optimal feedback control of dynamical systems via value-function approximation. *arXiv:2302.13122*, 2023.
- [20] Xingjian Li, Deepanshu Verma, and Lars Ruthotto. A neural network approach for stochastic optimal control. *arXiv:2209.13104*, 2022.
- [21] Victor G Lopez, Frank L Lewis, Yan Wan, Edgar N Sanchez, and Lingling Fan. Solutions for multiagent pursuit-evasion games on communication graphs: Finite-time capture and asymptotic behaviors. *IEEE Transactions on Automatic Control (TAC)*, 65(5):1911–1923, 2019.
- [22] Lu Lu, Raphael Pestourie, Wenjie Yao, Zhicheng Wang, Francesc Verdugo, and Steven G Johnson. Physics-informed neural networks with hard constraints for inverse design. *SIAM Journal on Scientific Computing*, 43(6):B1105–B1132, 2021.
- [23] Kjetil O Lye, Siddhartha Mishra, Deep Ray, and Praveen Chandrashekar. Iterative surrogate model optimization (ISMO): an active learning algorithm for PDE constrained optimization with deep neural networks. *Computer Methods in Applied Mechanics and Engineering*, 374:113575, 2021.
- [24] Volodymyr Mnih, Koray Kavukcuoglu, David Silver, Alex Graves, Ioannis Antonoglou, Daan Wierstra, and Martin A. Riedmiller. Playing atari with deep reinforcement learning. *arXiv*, 1312.5602, 2013.
- [25] Saviz Mowlavi and Saleh Nabi. Optimal control of PDEs using physics-informed neural networks. *Journal of Computational Physics*, page 111731, 2022.
- [26] Evgenii Nikishin, Pavel Izmailov, Ben Athiwaratkun, Dmitrii Podoprikin, Timur Garipov, Pavel Shvechikov, Dmitry Vetrov, and Andrew Gordon Wilson. Improving stability in deep reinforcement learning with weight averaging. In *Uncertainty in artificial intelligence workshop on uncertainty in deep learning*, 2018.

- [27] Derek Onken, Levon Nurbekyan, Xingjian Li, Samy Wu Fung, Stanley Osher, and Lars Ruthotto. A neural network approach for high-dimensional optimal control. *arXiv:2104.03270*, 2021.
- [28] Gianluigi Rozza, Andrea Manzoni, and Federico Negri. Reduction strategies for PDE-constrained optimization problems in haemodynamics. In *Proceedings of the 6th European Congress on Computational Methods in Applied Sciences and Engineering*, number CONF, pages 1748–1769. Vienna Technical University, 2012.
- [29] John Schulman, Filip Wolski, Prafulla Dhariwal, Alec Radford, and Oleg Klimov. Proximal policy optimization algorithms. *arXiv:1707.06347*, 2017.
- [30] David Silver, Aja Huang, Chris J. Maddison, Arthur Guez, L. Sifre, George van den Driessche, Julian Schrittwieser, Ioannis Antonoglou, Vedavyas Panneshelvam, Marc Lanctot, Sander Dieleman, Dominik Grewe, John Nham, Nal Kalchbrenner, Ilya Sutskever, Timothy P. Lillicrap, Madeleine Leach, Koray Kavukcuoglu, Thore Graepel, and Demis Hassabis. Mastering the game of go with deep neural networks and tree search. *Nature*, 529:484–489, 2016.
- [31] David Silver, Thomas Hubert, Julian Schrittwieser, Ioannis Antonoglou, Matthew Lai, Arthur Guez, Marc Lanctot, L. Sifre, Dharmashan Kumaran, Thore Graepel, Timothy P. Lillicrap, Karen Simonyan, and Demis Hassabis. A general reinforcement learning algorithm that masters chess, shogi, and go through self-play. *Science*, 362:1140 – 1144, 2018.
- [32] Maria Strazzullo, Francesco Ballarin, Renzo Mosetti, and Gianluigi Rozza. Model reduction for parametrized optimal control problems in environmental marine sciences and engineering. *SIAM Journal on Scientific Computing*, 40(4):B1055–B1079, 2018.
- [33] Richard S Sutton and Andrew G Barto. *Reinforcement learning: An introduction*. MIT press, 2018.
- [34] Fredi Tröltzsch. *Optimal Control of Partial Differential Equations: Theory, Methods and Applications*, volume 112 of *Graduate Studies in Mathematics*. 2010.
- [35] Sifan Wang, Mohamed Aziz Bhouri, and Paris Perdikaris. Fast PDE-constrained optimization via self-supervised operator learning. *arXiv:2110.13297*, 2021.
- [36] Jiajun Wu, Erika Lu, Pushmeet Kohli, Bill Freeman, and Joshua B. Tenenbaum. Learning to see physics via visual de-animation. In *NIPS*, 2017.
- [37] Mengfei Xu, Shufang Song, Xuxiang Sun, Wengang Chen, and Weiwei Zhang. Machine learning for adjoint vector in aerodynamic shape optimization. *Acta Mechanica Sinica*, pages 1–17, 2021.
- [38] Peng-Heng Yin, Guangqiang Xiao, Keju Tang, and Chao Yang. AONN: An adjoint-oriented neural network method for all-at-once solutions of parametric optimal control problems. *arXiv:2302.02076*, 2023.
- [39] Jiongmin Yong and Xun Yu Zhou. *Stochastic controls*, volume 43 of *Applications of Mathematics (New York)*. Springer-Verlag, New York, 1999. Hamiltonian systems and HJB equations.
- [40] Mo Zhou, Jiequn Han, and Jianfeng Lu. Actor-critic method for high dimensional static Hamilton–Jacobi–Bellman partial differential equations based on neural networks. *SIAM Journal on Scientific Computing*, 43(6):A4043–A4066, jan 2021.
- [41] Mo Zhou and Jianfeng Lu. A policy gradient framework for stochastic optimal control problems with global convergence guarantee. *arXiv:2302.05816*, 2023.
- [42] Hao Dong Zihan Ding. Challenges of reinforcement learning. In Shanghang Zhang Hao Dong, Zihan Ding, editor, *Deep Reinforcement Learning: Fundamentals, Research, and Applications*, chapter 7, pages 249–272. Springer Nature, 2020. <http://www.deeprreinforcementlearningbook.org>.

*DEPARTMENT OF MATHEMATICS, EMORY UNIVERSITY, ATLANTA, GA
Email address: dverma4@emory.edu

†DEPARTMENTS OF MATHEMATICS AND COMPUTER SCIENCE, EMORY UNIVERSITY, ATLANTA, GA
Email address: lruthotto@emory.edu

‡SANDIA NATIONAL LABORATORIES, ALBUQUERQUE, NM
Email address: {nwinovi, bartv}@sandia.gov